doi:10.1111/evo.13480

Evolution of cranial telescoping in echolocating whales (Cetacea: Odontoceti)

Morgan Churchill,[1,2,3] Jonathan H. Geisler,[1] Brian L. Beatty,[1] and Anjali Goswami[4]

[1]*Department of Biology, University of Wisconsin Oshkosh, Oshkosh Wisconsin 54901*

[2]*Department of Anatomy, College of Osteopathic Medicine, New York Institute of Technology, Old Westbury, New York 11568*

[3]*E-mail: churchim@uwosh.edu*

[4]*Life Sciences Department, The Natural History Museum, London SW7 5BD, United Kingdom*

Received December 19, 2017
Accepted March 23, 2018

Odontocete (echolocating whale) skulls exhibit extreme posterior displacement and overlapping of facial bones, here referred to as retrograde cranial telescoping. To examine retrograde cranial telescoping across 40 million years of whale evolution, we collected 3D scans of whale skulls spanning odontocete evolution. We used a sliding semilandmark morphometric approach with Procrustes superimposition and PCA to capture and describe the morphological variation present in the facial region, followed by Ancestral Character State Reconstruction (ACSR) and evolutionary model fitting on significant components to determine how retrograde cranial telescoping evolved. The first PC score explains the majority of variation associated with telescoping and reflects the posterior migration of the external nares and premaxilla alongside expansion of the maxilla and frontal. The earliest diverging fossil odontocetes were found to exhibit a lesser degree of cranial telescoping than later diverging but contemporary whale taxa. Major shifts in PC scores and centroid size are identified at the base of Odontoceti, and early burst and punctuated equilibrium models best fit the evolution of retrograde telescoping. This indicates that the Oligocene was a period of unusually high diversity and evolution in whale skull morphology, with little subsequent evolution in telescoping.

KEY WORDS: **Cranial telescoping, disparity, morphometrics, odontocete, oligocene, whale evolution.**

Over the course of their evolution, whales underwent massive morphological changes to adapt to aquatic environments (Fordyce and Muizon 2001; Gatesy et al. 2013; Marx et al. 2016). Among these changes, some of the most striking are changes to the architecture of the skull around the bony nares (Miller 1923; Heyning and Mead 1990; Klima 1999; Berta et al. 2014). In whales the external nares are displaced posteriorly, resulting in a foreshortening of the skull posterior to the rostrum, particularly the intertemporal region, as well as shortening of the nasals. Movement of the external nares coincides with posterior displacement and expansion of the premaxilla and maxilla, with the maxilla overlapping or underlapping the frontal, in a phenomena called cranial telescoping (Miller 1923). The term telescoping refers to a collapsible mariner's telescope, where long sections of telescope slide over shorter sections, in much the same way as whale facial bones slide over each other. This modification represents one of the most radical modifications of the mammalian skull, and alongside extreme cranial asymmetry, results in one of the most bizarre skulls possessed by any mammal (Berta et al. 2014). Possible explanations for cranial telescoping have included movement of the external nares to the top of the skull for easier breathing at the ocean surface (Raven and Gregory 1933; Whitmore and Sanders 1976; Heyning and Mead 1990; Klima 1999), bracing and support for a long rostrum (Miller 1923; Oelschläger 1990, 2000; Rauschmann et al. 2006), or evolution of novel behaviors and morphologies, such as filter-feeding in mysticetes (Berta et al. 2014), or echolocation in odontocetes (Oelschläger 1990; Rauschmann et al. 2006).

Cranial telescoping proceeds in two distinct patterns among cetaceans. In mysticetes (baleen whales), telescoping is dominated by the forward movement of posterior cranial elements (Miller 1923), here referred to as prograde cranial telescoping (Fig. 1B). The supraoccipital shield is displaced forward, in some

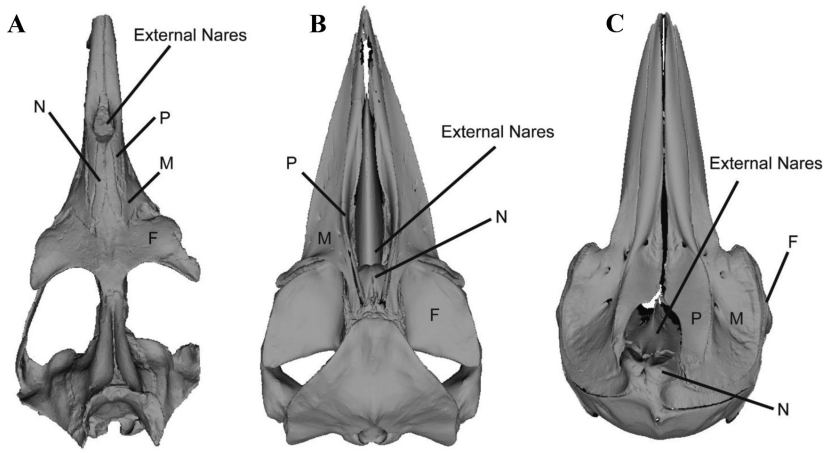

Figure 1. **Comparison of facial morphologies in archaeocete (*Zygorhiza kochi* USNM 11962), mysticete (*Balaenoptera acutorostrata* Reidenberg coll.) and odontocete (*Tursiops truncatus* USNM 571698) whales, based on 3d models. Premaxilla (P), maxilla (M), nasals (N), and frontal (F) indicated on skulls, as well as the location of the external nares.**

taxa as far as the orbit, leading to the parietal being almost or completely excluded from dorsal view. The nasal processes of the premaxilla and ascending processes of the maxilla expand posteriorly and approach the occiput, but narrow and taper posteriorly. By contrast the ventral portions of the maxillae expand posteriorly under the frontal to form a transversely wide infraorbital plate, which may limit further telescoping of anterior cranial elements.

Odontocetes (toothed or echolocating whales) have a more extreme pattern of cranial telescoping (Fig. 1C), here dominated by posterior expansion of anterior cranial elements (Miller 1923), which we refer to as retrograde cranial telescoping. In retrograde cranial telescoping, the frontals and maxillae expand in size and may contact the supraoccipital, completely eliminating the intertemporal region and largely excluding the parietal from dorsal view. The parietals may remain in the skull roof, but are covered (Whitmore and Sanders 1976), or become incorporated into the occiput (Geisler and Sanders 2003). The ascending process of the maxilla is expanded posteriorly as well as laterally, overlapping the frontal and leading to only a narrow wedge of the latter bone being exposed dorsally. Posterior development of the ascending process of the premaxillae also occurs, leading to some overlap of the maxillae. In one extinct odontocete clade, the Xenorophidae, the premaxillae are as transversely expanded as the maxillae, and the latter surprisingly underlies the latter (Geisler et al. 2014; Sanders and Geisler 2015).

All extant whales (Neoceti) show advanced degrees of telescoping. In contrast, no foreshortening of the intertemporal region or significant development and overlapping of frontals and maxillae has been documented in archaeocetes, even though posterior displacement of the external nares initiated prior to the origin of neocetes (Fig. 1A; Heyning and Mead 1990; Gatesy et al. 2013). Miller (1923), a detailed description of telescoping in whales, noted that telescoping was already far advanced in the few known early odontocetes. The only other study since then to describe in detail cranial telescoping was Whitmore and Sanders (1976), which focused on Oligocene whales. The absence of detailed quantitative studies of cranial telescoping in whales is rather surprising, in that this phenomenon is one of the most obvious trends to be observed in their evolution, and phylogenetic studies have incorporated telescoping related characters into phylogenetic analyses of both mysticetes and odontocetes (e.g.,Geisler and Sanders 2003; Fitzgerald 2010; Marx and Fordyce 2015; Churchill et al. 2016).

The goal of this study is to provide the first quantitative analysis of retrograde cranial telescoping in odontocetes. We integrate data from a diverse range of fossil and extant odontocetes, with an emphasis on Oligocene whale taxa. The Oligocene is a crucial time period in the evolution of whales, as it is during this epoch where we record the earliest known odontocetes and their initial diversification (Fordyce 1980; Fordyce and Muizon 2001; Geisler et al. 2014; Boessenecker et al. 2017). When Miller (1923) wrote his review of telescoping, only a few Oligocene odontocetes were known, but recent decades have resulted in the description of numerous new taxa (Fordyce 1994, 2002; Uhen 2008; Aguirre-Fernández and Fordyce 2014; Tanaka and Fordyce 2014; Boersma and Pyenson 2016; Churchill et al. 2016; Boessenecker et al. 2017). Thus in an attempt to better understand the evolution of cranial telescoping, we perform the first rigorous morphometric analysis of the facial region in fossil and extant odontocetes, with an emphasis on fossil odontocetes from the Oligocene Ashley and Chandler Bridge formations of South Carolina. These two formations have yielded numerous named and unnamed taxa (Fig. S1; Geisler and Sanders 2003) represented by well-preserved skulls that document numerous stages between the relatively untelescoped skulls of archaeocetes (i.e., stem cetaceans) and those of extant taxa (Whitmore and Sanders 1976; Geisler et al. 2014).

Inclusion of these important new fossils finally allows us to reassess the early evolution and diversification of cranial telescoping morphologies in odontocete whales.

Materials and Methods

SAMPLING

To examine morphological change in the facial region associated with telescoping, we collected 3D laser scans of 59 individual specimens representing 45 taxa (Appendix A). Taxon sampling emphasized odontocetes, but also included two archaeocetes, three toothed mysticetes, and one archaic baleen-bearing mysticete. Among odontocete whales, we included adult representatives of nearly every extant and recently extinct family, as well as many of their close fossil relatives. With the exception of a few rare species, all extant taxa are represented by 2–3 individuals, which were used to generate an average skull shape for subsequent morphometric analysis. The 34 fossil taxa are represented by single specimens, with an emphasis on the inclusion of material from the 24–29 Ma Ashley and Chandler Bridge formations of coastal South Carolina (Weems et al. 2016). Fossil taxa from these formations largely represent undescribed species, but include representatives of the Xenorophidae as well as species more closely related to crown group Odontoceti, including agorophiids, waipatiid, and squalodont-like species. Only fossil taxa with a well-preserved facial region were scanned. Five of these specimens were included because they had good preservation of the right but not left side of the skull. Analyses with these specimens were based on the right side only. All laser scan data was collected with a Creaform Handyscan 700 laser scanner, with files exported to .ply format at 0.2 or 0.5 mm resolution, except for *Odobenocetops peruvianus*, whose scan was downloaded from the Smithsonian X 3D website (https://3d.si.edu/), and *Chonecetus* sp., which was scanned with a FARO ScanArm. All fossil taxa were included within the analysis with no significant digital alteration, the exception being *Aetiocetus*, which had a damaged right frontal and squamosal. This damage was retrodeformed in the program Meshlab, by mirroring this portion of the skull on the intact left side, then inverting the copied portion and merging it with the damaged region. All other taxa included within this analysis had fairly complete crania for the right side of the skull.

We have archived .stl files of all USNM, ChM, SDSNHM, GSM, and select CCNHM specimens used in this analysis to the phenome10k website (http://phenome10k.org/). For a list of specific specimens uploaded, please see Appendix A.

GEOMETRIC MORPHOMETRICS

To capture the variation in morphology associated with retrograde telescoping, we used a landmark and sliding semilandmark approach on the facial region of the skull, rather than the entire skull. This allowed us to maximize the sampling of fossil taxa, many of which possessed considerable damage to the rostrum, basicranium, or squamosals. Specifically we performed landmarking on the intertemporal region, nasals, and the portion of the face (frontal, maxilla, and premaxilla) posterior to the antorbital notch.

A total of 26 landmarks (Table 1) and 314 semilandmarks were placed on digital models of the skulls (Fig. 2), using the program IDAV landmark (Wiley et al. 2005). A sliding semilandmark approach (Bookstein 1997; Gunz et al. 2005) was chosen due to the complexity of shape present within whale skulls, which cannot be captured using traditional landmarking methods. These semilandmarks were used to define curves representing the shape of specific cranial bones in the facial region for each side of the skull. To accommodate the five specimens that had damage to the left side of the skull, a second set of landmark files was created, where only landmark data from the right side of the skull and midline was included. This analysis included all the taxa from the whole skull analysis, as well as *Diorocetus hiatu*s, *Eurhinodelphis longirostris*, *Odobenocetops peruvianus*, *Xenorophus* n. sp. (ChM PV4823), and *Xiphiacetus cristatus*.

Although the landmarks chosen for our morphometric analysis generally performed well across the disparate skull morphologies in our sample, radical skull modification in some lineages as well as major differences in cranial shape between odontocetes and other whales presented particular challenges with some landmarks of the nasals, intertemporal region, and antorbital notch. Nasals are completely absent in *Kogia* (Schulte 1917), so to include this taxon in our analysis we overlapped all six nasal landmarks at the intersection of the posterior margin of the external nares and the nasal septum, where nasals are situated in other cetaceans. In other taxa the anterolateral border of the nasals does not contact the maxilla. In these cases, the curves defining the borders of the maxilla were extended to the anterolateral border of the nasals, by following the premaxilla/frontal suture to the nasals. In the case of the intertemporal region, the parietal is almost completely excluded from dorsal view in crown odontocetes, preventing precise landmarking of the occipital-parietal and parietal-frontal sutures. To accommodate this morphological change, both landmarks were placed closely together and overlapping, at the approximate dorsal apex of the temporal crest where the occipital shield, temporal wall, and facial region all intersect. Finally, there are substantial differences in the shape and form of the antorbital notch in archaeocete and mysticete whales in comparison to the morphology observed in odontocetes. In the former two clades, landmarks for the antorbital notch were placed on the lateral margin of the ascending process of the maxilla, at a position at level with the anterior edge of the frontal in dorsal view, to ensure comparability of landmarks between all three groups

Table 1. Landmarks used in morphometric analysis of the whale skull.

Landmark #	Description
1	**Anterior margin of nasals on suture between right and left nasals**
2	**Posterior margin of nasals on suture between right and left nasals**
3	**(Approximate) position of parietal-frontal suture on midline**
4	**Apex of occipital shield near or on the midline of the skull**
5	Anterior edge of posteriormost infraorbital foramen
6	Antorbital notch on maxilla
7	Anterolateral corner of nasal
8	Posterolateral corner of nasal
9	Lateral edge of the posterior terminus of the ascending process of the premaxilla
10	Anteromedial corner or border of the external nares, on the premaxilla
11	Lateral border of the premaxilla, at point where premaxilla forms an angle between the rostrum and the face
12	Anteroventral border of the supraorbital process of the frontal
13	Posteroventral border of the supraorbital process of the frontal
14	Parietal-occipital suture on the dorsal border of the temporal fossa or sagittal crest
15	Parietal-frontal suture on the dorsal border of the temporal fossa or sagittal crest
C1	Semilandmark curve representing the posterior margin of frontal at the midpoint to anterior edge of supraorbital process of the frontal
C2	Semilandmark curve representing the posterior margin of the maxilla from the posterolateral margin of maxilla at or near contact with nasal to antorbital notch
C3	Semilandmark curve representing the posterior extension of the premaxilla from the lateral margin of premaxilla at point of inflexion with face to anteromedial border of external nares

Landmarks in bold represent single points on the midline, while nonbolded landmarks represent paired points present on both sides of the skull. Curves indicated by a C preceding the number. See Figure 2 for further information.

of whales. Examples of landmarking for these more problematic taxa are illustrated in Figure S2.

After the completion of initial landmarking in IDAV, a sliding procedure with thin spline deformation was performed iteratively on the semilandmarks in the R package "Morpho" (Schlager 2017), until the bending energy of the thin spline deformation is minimized. During this procedure, semilandmarks are allowed to slide along the predefined curves, creating comparable landmarks that can be used to quantify shape variation. The generated landmarks and semilandmarks were then analyzed using Procrustes superimposition, with Principal Components Analysis (PCA) performed on the resulting Procrustes coordinates, in the R package "geomorph" (Adams and Otarola-Castillo 2013). Scree plots were used to then identify the point where additional components explain very little variance, and modeled extreme skull shapes (minimum and maximum) were created to determine the nature of shape variation by each component. All Procrustes superimposition and PCA were performed in the R package "geomorph," with the R code used to slide the semilandmarks presented in Appendix B.

PHYLOGENETIC ANALYSES

The phylogenetic relationships of many of the specimens and taxa we have scan data for are unknown. Thus to analyze patterns of evolution in cranial telescoping, we first had conduct a phylogenetic analysis that included all the taxa analyzed in the geometric morphometric analysis. To accomplish this, we started with the supermatrix of Lambert et al. (2017), and then added 10 specimens that were scanned, but could not be assigned to any named taxon, as well as *Schizodelphis morckhoviensis* (USNM 13873), a different but uncertain species from the same genus (*Schizodelphis* sp.; CCNHM 141), *Eurhinodelphis longirostris* (USNM 244404), *Odobenocetops peruvianus* (cast of SMNK PAL 2491), *Odobenocetops leptodon* (SAO 202, cast of SMNK PAL 2492), and *Lagenorhynchus albirostris* (USNM 35156, 267563, 504659, 504660). The resulting supermatrix has 327 morphological characters, 60,850 molecular characters, and 121 operational taxonomic units. Relationships among extant taxa were constrained based on Bayesian analysis of the molecular data as reported in three previous studies (McGowen et al. 2009; Geisler et al. 2011; McGowen 2011). All relationships among extant taxa were resolved in the constraint, except for a trichotomy within Ziphiidae that leads to *Ziphius cavirostris*, *Tasmacetus shepherdi*, and *Mesoplodon* spp. A backbone constraint was used where all extinct taxa were designated as floaters; this meant that extinct taxa could be placed within constrained clades of extant taxa without violating those constraints. The most parsimonious tree was recovered using the application TNT (Goloboff et al. 2008). Specifically a new

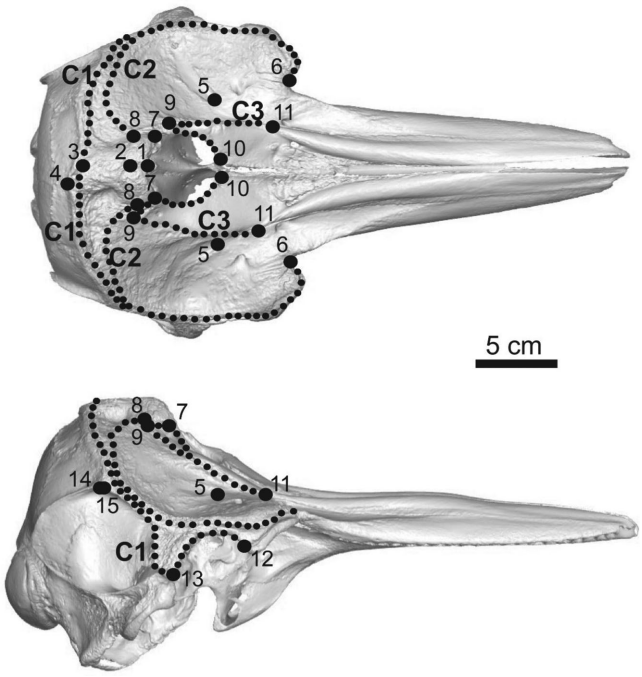

Figure 2. Landmarks and semilandmarks used in morphometric analysis of the cranial region, on a 3d model of the skull of *Tursiops truncatus* (SDNHM 11102). Landmarks are indicated by large black circles labeled by number, while semilandmarks are labeled as C1, C2, and C3, and demarcated by small black circles. Semilandmarks on figure do not represent actual number of semilandmarks used during landmarking, but only represent the outline of features landmarked.

technology search was employed with all default settings except that the shortest tree was found 1000, instead of 100, times.

Support values were determined with a bootstrap analysis as executed in TNT; 100 bootstrap replicates were conducted with replacement. Default values and selections were used except as follows: (1) absolute frequencies, instead of frequency differences, were used; (2) shortest trees for each replicate were found using 50, not 10, random taxon addition sequences followed by TBR swapping. Constraints were enforced as described above, but given that extinct taxa were defined as floaters, many of the constrained nodes have a frequency $< 100\%$.

The phylogenetic positions of four specimens were determined based on previous phylogenetic analyses that included different specimens of what are likely the same species or genus. Justification for their placement in the phylogeny is described in the supplementary material, with comparisons of the skulls included provided in Figure S3. Results of phylogenetic analyses are presented in Figures S4 and S5.

PGLS AND ALLOMETRY

Allometry may have a significant influence on shape, and to assess the impact of allometry on the results of the PCA, we used PGLS to assess the correlation of significant components with bizygomatic width of the skull (BIZYG), a reliable proxy for body size (Pyenson and Sponberg 2011). PGLS was used instead of regular least squares regression to correct for the influence of phylogeny, as data points are not statistically independent but share common ancestries (Felsenstein 1985). These regressions were performed only on the whole skull dataset, as these taxa were represented by more complete specimens than those only landmarked for half the face.

We used the novel phylogeny produced by our phylogenetic analysis as outlined above for the PGLS. All taxa not included within the morphometric analysis or with missing BIZYG measurement data were pruned from the tree for use in the PGLS.

To incorporate branch length data into our PGLS, we time-calibrated our phylogeny using fossil age information binned by stage (Appendix E). Age data for whale taxa were gathered from the Paleobiology Database (https://paleobiodb.org), with age data for undescribed Oligocene taxa gathered from museum records. This was carried out using the "paleotree" package in R (Bapst 2012). Time calibration was performed using the "equal" method, allowing extension of branches of zero length so that they share time equally with the first preceding branch, with a vartime value of 2 million years used to calibrate the root of the tree. The resulting time-calibrated tree was then visually checked to determine if there were any problematic reconstructed divergence times, either unrealistically old or unrealistically young. Regression analyses were carried out using the "nlme" and "APE" packages (Paradis et al. 2004) in R, using a maximum likelihood method. Strength of regression was assessed using a combination of AIC_c scores and P values (P values less than or equal to 0.05 were considered significant).

ANCESTRAL CHARACTER STATE ANALYSIS

To determine how the morphology of the facial region evolved, we performed Ancestral Character State Reconstruction (ACSR) on those single principal components that explained the most variation (44.63% for the right side of the skull, and 49.26% for the whole skull) and reflected morphological change associated with cranial telescoping. To do this, we constructed phylomorphospaces that plot the PCA scores against a phylogeny, as implemented in the R package "geomorph" and using the time-calibrated phylogeny used in our PGLS analyses.

Prior to this however, we first tested for phylogenetic signal, using physignal in "geomorph" and the "Kmult" method (Adams 2014) with 1001 random permutations. If no phylogenetic signal was evident in our dataset, further ACSR would be unwarranted. We also performed a separate ACSR on centroid size, treating this variable as a continuous character. Centroid size is the square

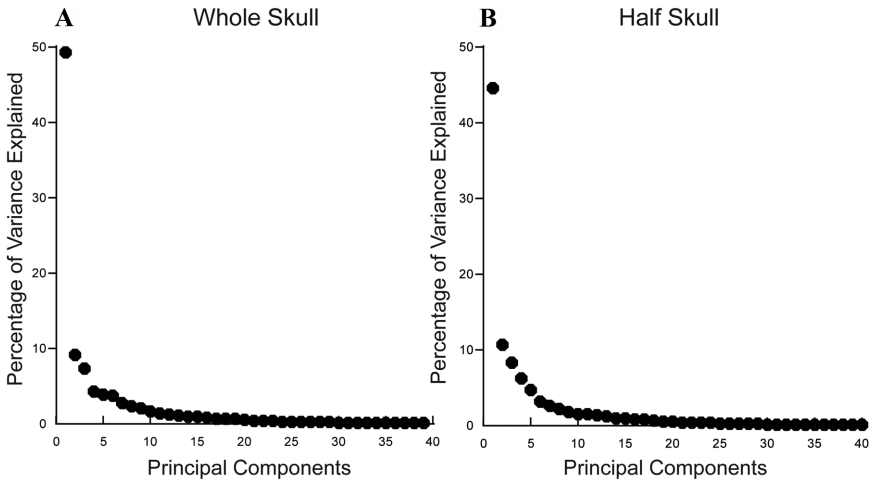

Figure 3. Scree plots comparing percentage of variance with principal components, for whole (A) and half skull (B) principle component analyses.

root of the sum of the squared distances for each landmark point from the centroid, and is typically used as a proxy for body size in a geometric morphometric data set. However, given the radical modification of the cetacean skull and the substantial change in relative size of the maxilla and frontal, centroid size may instead be an accurate proxy for change in the expansion of the frontal and maxilla, related to telescoping. We performed ACSR on centroid size data from the half and whole facial region datasets, using the time-calibrated phylogeny referenced above. This ACSR was implemented using the contMap function in the R package "phytools" (Revell 2012).

MODEL OF EVOLUTION

We were also interested in determining what evolutionary models may best explain the patterns of evolution observed in our dataset. For these analyses, we tested the fits of different models of evolution for principal components related to telescoping, as well as centroid size, using the time-calibrated tree produced for the ACSR analyses. Models of evolution were fit for individual PCs in the R package "geiger" (Harmon et al. 2008), using 100 random starting points and a AIC_c criteria to assess which model best fits the trait data. Five models of evolution were tested: Brownian motion (Felsensein 1973), which tests whether a random walk best explains the pattern of evolution observed; Ornstein-Uhlenbeck (Butler and King 2004), which fits a random walk with a central tendency; Early Burst (Harmon et al. 2010), which assumes that the rate of evolution increases or decreases through time; time-dependent or delta model (Pagel 1999), where rate of evolution varies over time, and punctuated equilibrium or kappa, where rates of evolution increase during major bouts of speciation (Pagel 1999).

Results

MORPHOLOGICAL VARIATION AND ALLOMETRY

In the analysis in which only the right side of the skull was analyzed, 20 components are needed to explain 95% of the variance observed in the facial region; a scree plot (Fig. 3A) identifies the first six components as each explaining significant variation (cumulative ~77%). Principal component one explains 44.63% of the variation and reflects posterior migration of the external nares and premaxilla, expansion of the maxilla and frontal, shortening of the nasals, and elimination of the intertemporal region from dorsal view. Five distinct clusters of points can be observed (Fig. 4A), which appear to segregate taxa by degree of cranial telescoping, with PC1 scores increasing with degree of telescoping. Archaeocetes have the most negative PC1 scores, and toothed mysticetes form a cluster distinct from archaeocetes with somewhat more positive PC 1 scores, between –0.6 and 0.4. The baleen-bearing whale *Diorocetus* plots separately from the toothed mysticetes, within the gap between toothed mysticetes and xenorophids, being somewhat closer to xenorophids.

A large gap in PC1 scores separates odontocetes from other whales. Two clusters of odontocete whales can be readily distinguished; a cluster with negative PC1 scores between approximately –0.2 to 0, comprising xenorophids, agorophiids, and simocetids; and a cluster comprising crown Odontoceti, as well as waipatiid and squalodont-like stem odontocetes, which all possess positive PC1 scores. The one exception is the fossil crown group odontocete *Odobenocetops,* which overlaps in morphospace with xenorophids along PC1.

Principal component 2 (Fig. 4A) explains 10.68% of the variation and represents shape of the external nares as well as lateral expansion of the skull and anteroposterior position of the orbit. Taxa with negative PC scores possess relatively wide skulls

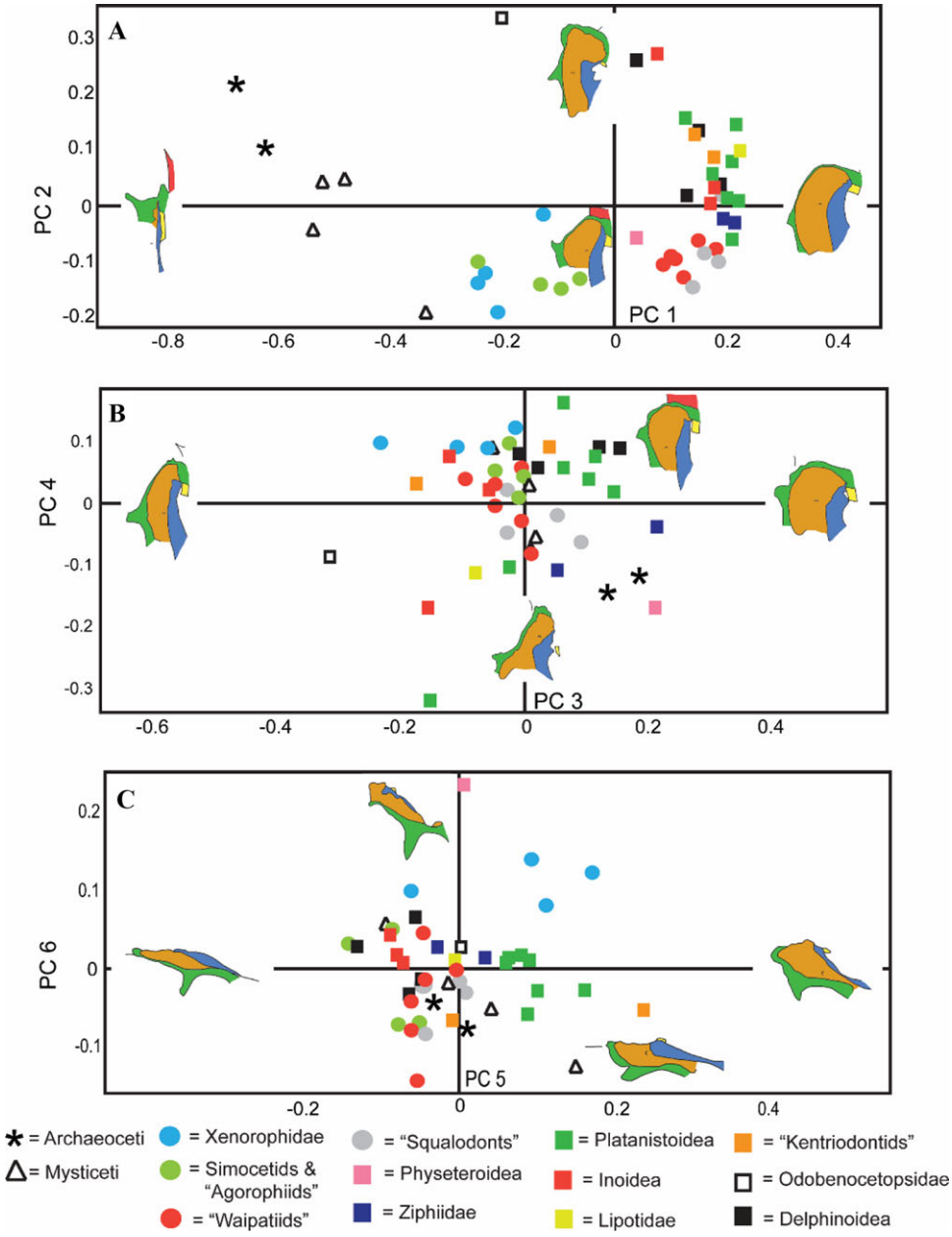

Figure 4. Results of the PCA analysis of the right half of the facial region, showing plots of PC 1 versus 2 (A), PC 3 versus 4 (B), and PC 5 versus PC 6 (C). Skulls illustrated represent hypothetical modeled extremes indicating the morphological change associated with each principal component analysis. Coloring on bones: parietal, red; premaxilla, blue; maxilla, orange; nasals, yellow; and frontal, green. Crown group odontocetes are represented by squares, while stem taxa are represented by circles.

with posteriorly placed orbits and an "open" external nares that grades into the mesorostral groove of the rostrum. Taxa with positive PC scores have narrower skulls with anteriorly placed orbits, greater overlap of frontal and maxilla, increased asymmetry in the premaxilla, and heart-shaped, constricted external nares. This PC axis largely segregates crown group odontocete from stem odontocete taxa, with stem taxa having the more negative PC2 scores. *Odobenocetops* possesses the highest PC 2 score, plotting apart from other crown group odontocetes. Archaeocetes and toothed mysticetes overlap in morphospace with crown group odontocetes on PC2.

Principal component three (Fig. 4B) explains 8.27% of the variation and reflects overall proportional width and length of the facial region, in particular the middle portion of the face. Segregation on this axis is poor, although in general stem odontocetes show narrower skulls and more negative PC3 scores than most crown group taxa. Principal component four (Fig. 4B) explains 6.3% of the variation and represents anterolateral development of

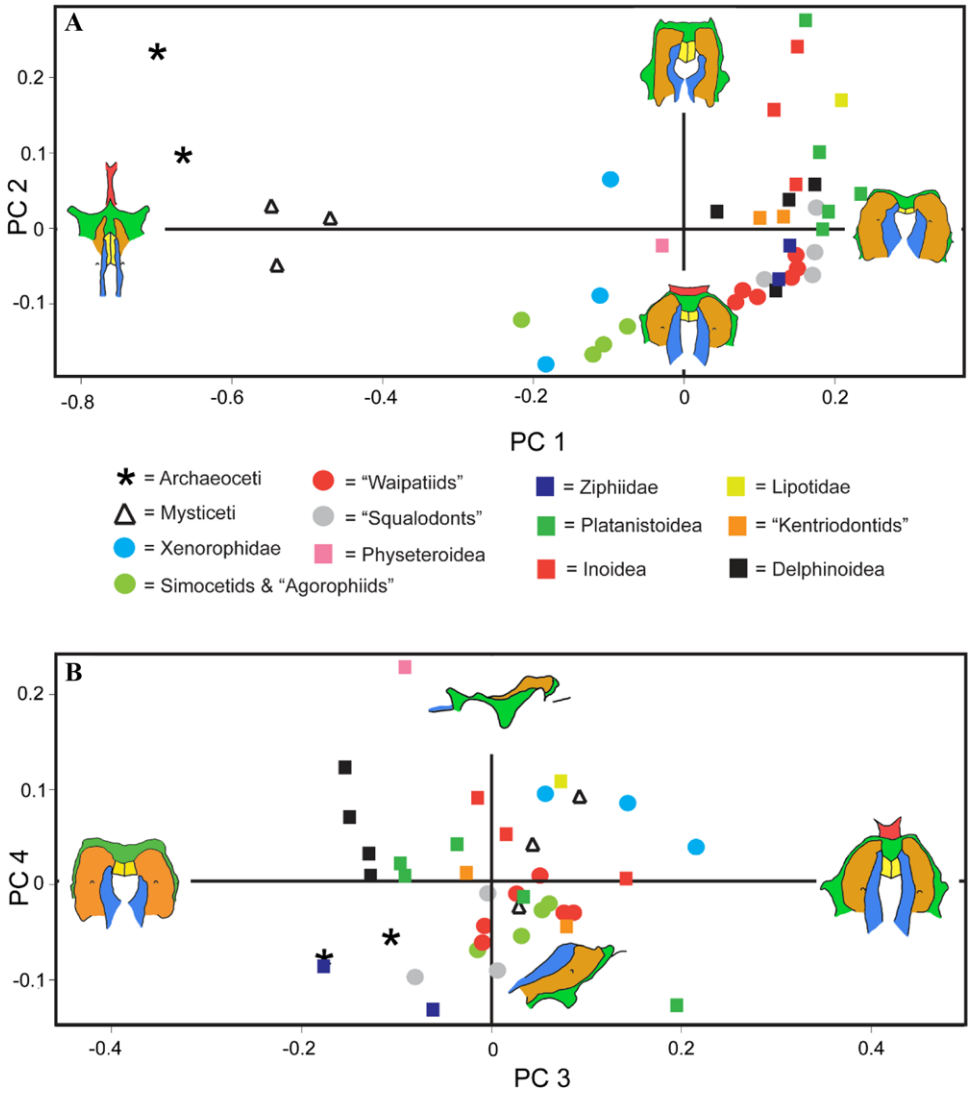

Figure 5. Results of the PCA analysis of the whole facial region, showing plots of PC 1 versus 2 (A) and PC 3 versus 4 (B). Skulls illustrated represent hypothetical modeled extremes illustrating the morphological change associated with each principal component analysis. Coloring on bones: parietal, red; premaxilla, blue; maxilla, orange; nasals, yellow; and frontal, green. Crown group odontocetes are represented by squares, while stem taxa are represented by circles.

the frontal and orbit size, with taxa with more negative scores having more anterolaterally positioned small orbits. A large degree of overlap in morphospace occupation is seen for this PC, with archaeocetes, *Kogia*, *Platanista*, and *Inia* having more negative scores than most taxa. Principal component five (Fig. 4C) explains 4.74% and reflects dorsoventral development of the skull toward the midline. Generally speaking, positive PC scores reflect increased convexity and somewhat distinguish xenorophids, platanistoids (sensu Churchill et al. 2016), and *Odobenocetops* from other taxa, while taxa with more negative scores have overall flatter skulls. Finally, PC6 (Fig. 4C) explains 3.21% of the variation seen in the facial region, with positive PC6 scores representing a more dorsoventrally developed skull with larger postorbital processes and greater facial concavity. This PC separates *Kogia*, and to a lesser extent Xenorophidae, from all other taxa.

In the analysis where the whole facial region was analyzed, 19 components are needed to explain 95% of the variance observed in the facial region; a scree plot (Fig. 3B) identifies the first four components as each explaining significant amounts of variation (~70%). Principal components one and two (Fig. 5A) explain 49.26% and 9.14% of the variation respectively, and show the same overall pattern as found in the analysis of the right side of the skull for taxa represented in both analyses (Fig. 4A). Patterns in morphological variation observed for PC3-4 for whole skulls differ from those seen for the right half of skulls, largely as a result of the deletion of taxa included within the half skull analysis. Principal component 3 (Fig. 5B) represents 7.38% of the

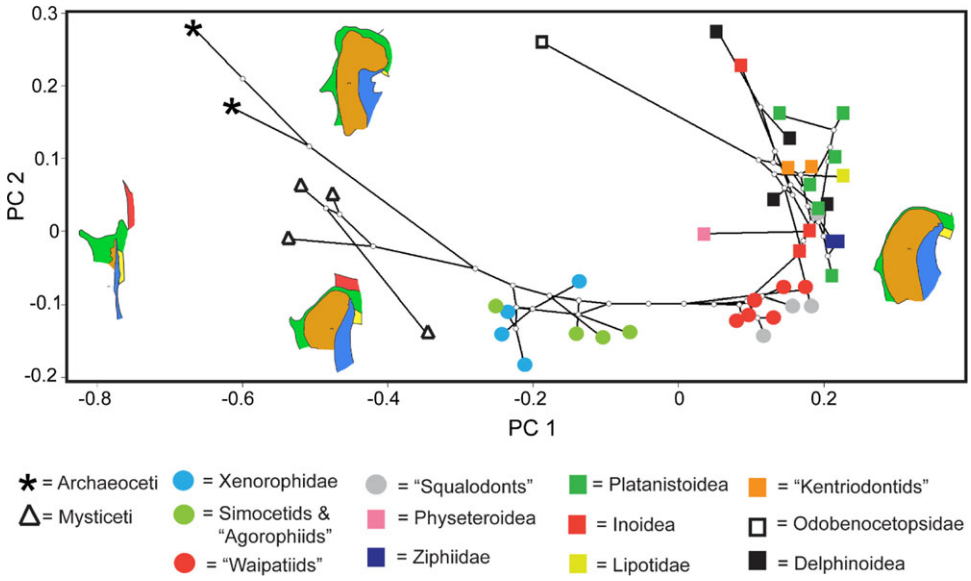

Figure 6. **Phylomorphospace for the half skull dataset, using the topology recovered in our phylogenetic analysis (Figs. S4 and S5) and with time-calibrated branch lengths based on data in Appendix E. Skulls illustrated represent hypothetical modeled extremes indicating the morphological change associated with each principal component analysis. Coloring on bones: parietal, red; premaxilla, blue; maxilla, orange; nasals, yellow; and frontal, green. Crown group odontocetes are represented by squares, while stem taxa are represented by circles.**

variation, and reflects the width of the intertemporal region and posterior portion of the face. Broad overlap of taxa occurs along this axis, but delphinoids, kogiids, and ziphiids (with relatively broad posterior facial regions) are segregated from taxa with relatively narrow posterior facial regions, such as xenorophids and some river dolphins. Principal component four (Fig. 5B) explains 4.32% of the variation, and largely represents the concavity of the skull, with taxa with highly concave skulls having very positive PC4 scores, while more negative scores represent convex skulls. There is broad overlap in PC4 scores for different whale clades, although *Kogia* has a positive PC4 score clearly separating this taxon from all other whales.

PGLS analysis indicates no significant correlation of PC 1 ($P = 0.60$), PC 2 ($P = 0.69$), or centroid size ($P = 0.13$) with body size. This indicates that allometry does not play a significant role in influencing the facial morphology of whales, and that centroid size recovered from morphometric analysis is rather a function of the growth and change in shape of the maxilla and frontal, not an increase in body size.

ANCESTRAL CHARACTER STATE ANALYSIS

Significant phylogenetic signal was found for both the whole skull ($K = 1.8$, $P = 0.001$) and half skull morphometric datasets ($K = 1.49$, $P = 0.001$). Given that PC 1 and to a lesser extent, PC 2, seem to best capture the morphological variation associated with cranial telescoping, we only constructed a phylomorphospace for these components. Furthermore, given the near identical patterns recovered between analyses of whole and half skulls, only the phylomorphospace for the half skull dataset (Fig. 6) is presented here, as it includes the largest taxonomic sample.

Large increases in PC 1 scores are recovered through the base of our phylogeny. We reconstruct a higher but still negative PC 1 score as the ancestral condition for Neoceti (odontocetes + mysticetes; –0.28) and a somewhat less negative PC 1 score as the ancestral condition for Odontoceti (–0.22). These scores are less negative than the reconstructed PC 1 score for Mysticeti (–0.42). Along the stem of Odontoceti, successive increases in PC 1 are found up to the clade comprising waipatiid and squalodont like taxa, as well as all later diverging odontocetes (0.12), with a further increase at the base of crown Odontoceti (0.17). Within crown Odontoceti, ancestrally reconstructed PC 1 scores range from 0.11 to 0.21, without clear evolutionary trends.

For PC 2, high PC 2 scores are found toward the base of the whale phylogeny (0.15–0.7), with very low PC 2 scores recovered at the base of Neoceti (–0.07). From the base of Odontoceti through the emergence of crown Odontoceti, reconstructed PC 2 scores occupy a very narrow region of the morphospace (–0.08 to –1.0). Major increases in PC 2 scores can be seen at the base of crown Odontoceti (0.09), after which a great degree of variation can be seen in PC 2 scores.

Ancestral state reconstruction of centroid size (Fig. 7) indicates large increases in centroid size at the base of Pelagiceti (Basilosauridae + Neoceti), Neoceti, and Odontoceti, with mysticetes and archaeocetes having small centroid sizes despite their

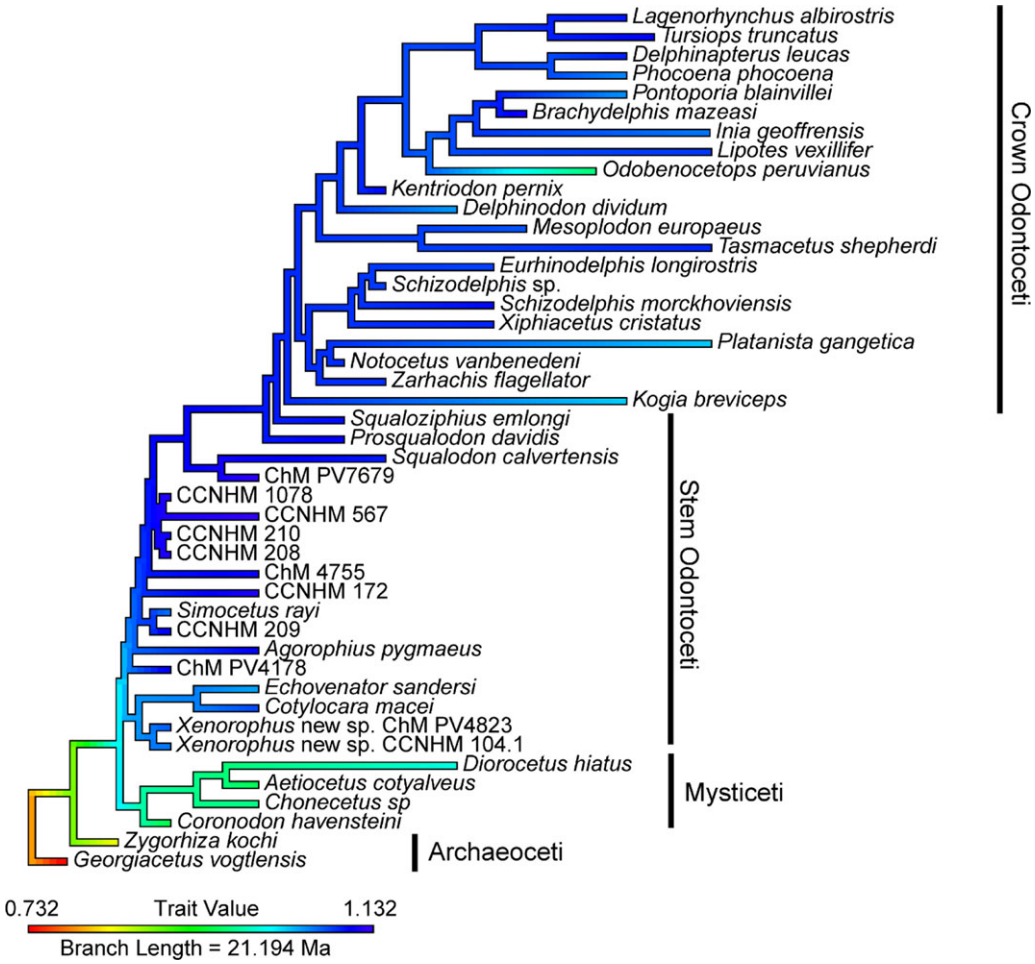

Figure 7. **Ancestral character state analysis of centroid size from analysis of half skulls, based on the tree topology recovered from our phylogenetic analysis (Figs. S4 and S5) and time-calibrated using age information presented in Appendix E.**

relatively large body size. Centroid size exhibits minor variation within Odontoceti, although a slight increase for centroid size is reconstructed at the base of a clade comprising ChM PV4178 and all later diverging odontocetes. Ancestral state reconstructions of centroid size in the whole skull dataset are nearly identical and not presented here.

MODEL OF EVOLUTION

The model that best fits the evolution of PC1 scores was the punctuated equilibrium model, which had the lowest AIC_c score of any model (Table 2), although not significantly different from the score for the early burst model, suggesting that this model also fits the pattern of evolution observed. For PC 2, the time dependent model was best supported. However, the AIC_c score for the early burst model was only slightly higher and not significantly different, suggesting both models equally explain the patterns observed for PC 2. The early burst model of evolution best fits centroid size evolution, with an AIC_c score far lower than that reported for any other model.

Discussion

EVOLUTION OF THE ODONTOCETE SKULL

Our study is the first to quantify the morphological change in facial shape and retrograde telescoping in fossil and living odontocetes, and we discovered several unrecognized patterns in the evolution of the cetacean skull. Principal component one, which explains the majority of the variation in the cetacean facial region, is associated with many of the hallmark features of cranial telescoping, including expansion of the maxilla and frontal and compression of the intertemporal region. When PC1 is placed in a phylogenetic context, we can see that an advanced condition of cranial telescoping is already evident at the base of Neoceti. This suggests that cranial telescoping may have slightly reversed along the mysticete stem, and that the common ancestor of neocetes may have more closely resembled an odontocete whale than a toothed mysticete. Alternatively, given our limited sample size of mysticetes and archaeocetes, this reconstructed state could be an artifact of heavier sampling of odontocetes, and inclusion of additional early baleen whales, such as *Llanocetus* (Mitchell 1989)

Table 2. Results of tests of model of evolution, for PC 1, PC 2, and centroid size.

	PC 1			PC 2			Centroid size		
Model	Log likelihood	AIC_c	Parameter	Log likelihood	AIC_c	Parameter	Log likelihood	AIC_c	Parameter
Brownian motion random walk	16.08	–27.83	σ2 = 0.004 z0 = –0.63	41.87	–79.41	σ2 = 0.001 z0 = 0.16	53.27	–102.22	σ2 = 0.001 z0 = 0.78
Ornstein–Uhlenbeck	16.11	–25.55	α = 0.002 σ2 = 0.004 z0 = –0.62	43.05	–79.44	α = 0.025 σ2 = 0.001 z0 = 0.15	53.48	–100.3	α = 0.004 σ2 = 0.001 z0 = 0.78
Early burst	32.20	–57.74	α = –0.13 σ2 = 0.015 z0 = –0.62	44.05	–81.44	α = –0.04 σ2 = 0.002 z0 = –0.62	**73.20**	**–139.73**	**α = –0.14** **σ2 = 0.002** **z0 = 0.79**
Time dependent	26.38	–46.1	δ = 0.09 σ2 = 0.008 z0 = –0.59	**45.30**	**–83.93**	**δ = 0.42** **σ2 = 0.001** **z0 = –0.14**	69.85	–133.03	δ = 0.07 σ2 = 0.001 z0 = 0.81
Punctuated equilibrium	**32.40**	**–58.11**	***k* = 0** **σ2 = 0.004** **z0 = –0.64**	42.64	–78.61	*k* = 0.68 σ2 = 0.001 z0 = 0.16	63.96	–121.26	*k* = 0 σ2 = 0.001 z0 = 0.78

σ2, Brownian motion rate parameter; α, strength of pull toward optimum in Ornstein–Uhlenbeck; *k*, exponent branch lengths are raised by in punctuated equilibrium; δ, rate of recent evolution; z0, root state. Model with lowest AIC_c scores for each variable in bold.

and the recently described *Mystacodon* (Lambert et al. 2017b), is needed to decipher the degree of cranial telescoping in the earliest known neocetes. Furthermore, although our sampling is too limited to draw firm conclusions, a distinct trend in increased retrograde telescoping is recovered within mysticetes as well. This occurs despite the fact that prograde telescoping, which is not examined here, is overall considered to be the dominant form of telescoping within mysticetes (Miller 1923).

Our study also confirms that cranial telescoping was already far advanced in the earliest known odontocetes, in agreement with Miller (1923) and Whitmore and Sanders (1976). In mysticetes, a variety of transitional taxa are preserved ranging from whales little differentiated from their archaeocete ancestors (e.g., *Mystacodon* (Lambert et al. 2017b), and *Coronodon* (Geisler et al. 2017)), to the baleen whales of today (Marx and Fordyce 2015). In contrast, the oldest known odontocete whales display clear morphological features of the suborder (Uhen 2008), and possess many of the traits we associate with toothed whales today, including ultrasonic hearing (Churchill et al. 2016; Park et al. 2016) and echolocation (Geisler et al. 2014). Associated with the early emergence of these traits is the evolution of advanced retrograde telescoping.

This rapid evolution of retrograde telescoping in odontocetes is supported by our statistically significant fit of the early burst model to the pattern of evolution for cranial telescoping-related principal components. While our punctuated equilibrium model was also found to fit the pattern observed in telescoping evolution, the emphasis in our analyses on Oligocene whales may be resulting in the identification of the Oligocene as a period of high speciation relative to later time periods, and resulting in inaccurate model results. One should note that we are also still likely missing several million years of early odontocete evolution, given that Eocene odontocetes are as of yet unknown, in contrast to mysticetes (Lambert et al. 2017b; Mitchell 1989). Still, based on the available fossil record, retrograde cranial telescoping evolved fast and early at the base of the odontocete phylogeny, with neither minimal evolution nor a clear directionality post-Oligocene.

Although the oldest known odontocetes already show some degree of cranial telescoping, the fossil record allows us to identify three major grades in the evolution of facial morphology and cranial telescoping in early odontocetes. The first grade is represented by Xenorophidae, *Simocetus*, *Agorophius*, and undescribed taxa closely related to them. In these taxa, the external nares, nasals, and ascending process of the premaxilla are slightly anterior to the orbits or level with their anterior portions, in a posterior position as compared to toothed mysticetes and archaeocetes. Associated with this displacement is posterior expansion of the maxilla and frontal, with the former broadly overlapping the latter. However, lateral expansion of the maxilla is limited, the intertemporal region is broadly exposed dorsally, and the nasals are long. The expansion of the posterior portion of the maxilla, which in extant odontocetes serves as the origin for hypertrophied and differentiated facial muscles that control the production of high frequency clicks and whistles at the phonic lips, suggests that the ability to create these sounds in the face had

already evolved, consistent with the findings from other studies (Fordyce 2002; Geisler et al. 2014). The anterior position of the bony nares, as compared to extant odontocetes, suggests that the melon, if present, was much smaller. By contrast anteriorly positioned nares increases the length of the nasal passages, leaving ample space for olfactory turbinals. In fact, turbinals have been found in taxa of this grade (Boessenecker et al. 2017), as well as in one for which the nares are more posteriorly positioned (Godfrey 2013). The second phase of evolution in cranial telescoping is present in later diverging stem-odontocetes including probable waipatiid- and squalodont-like taxa. In these species, we see further posterior displacement of the external nares, either level with or slightly posterior to the orbits, associated with posterior movement of surrounding cranial elements. This would not only suggest that the blowhole was positioned more dorsally on the head, but would allow for a larger nasal apparatus and melon for echolocation. Nasals are foreshortened anteroposteriorly, and the intertemporal region is almost completely eliminated from dorsal view. Small parietal triangles may be seen on the lateral margins of the reduced intertemporal region, or the parietals may be completely covered by the frontals and maxillae (Whitmore and Sanders 1976). Phylogenetic relationships within this section of the whale tree are still hotly contested, particularly whether squalodonts and waipatiids are outside the crown group (Lambert et al. 2014; Lambert et al 2015; Churchill et al. 2016), as recovered in our analysis, or within a more broadly inclusive Platanistoidea (Tanaka and Fordyce 2015; Boersma and Pyenson 2016; Tanaka and Fordyce 2017). If the later hypothesis is true, this might suggest that further developments in retrograde telescoping evolved convergently in platanistoids and Delphinida.

The final phase of cranial telescoping can be seen in crown odontocetes. This grade is characterized by transverse narrowing of the skull leading to increased overlap of the frontal and maxilla. This phase of telescoping is reflected in PC 2 scores; although there is a great deal of variability in these scores within modern odontocetes, all living taxa show higher PC2 scores than those exhibited by "squalodonts" and earlier diverging taxa. Generally, this appears to be associated with a potential increase in the diameter of the nasal air sacs, facial musculature, and the melon (especially its aperture), even for animals of relatively small body size. The size of the aperture of the melon, which is its width where makes it closest approach to the skin, appears to be linked to the range of wavelengths that can propagate from the melon to the environment (Au et al. 2006; McKenna et al. 2012), and the explosive diversification of modern odontocetes could have been driven by the broadened sensory range enabled by a broader melon.

Within the crown group, with the exception of *Odobenocetops*, very little variation in PC 1 scores is observed. Subsequent principal components appear to largely represent transverse and dorsoventral development of the facial region. This suggests that modification of the skull associated with retrograde cranial telescoping provides a strong functional constraint on further modification of the skull in that aspect. To produce the diversity of facial form found in crown odontocetes, as seen in PC 2 and subsequent components, cranial proportions could largely only be altered in the transverse plane, or by increasing or decreasing the convexity of the skull. Furthermore, while a clear phylogenetic structure is evident in PC 1 for stem taxa, crown group odontocete clades do not cluster into discrete groups with distinct facial morphologies.

Our analyses show an increase in PC 1 scores and cranial telescoping along the stem of odontocete whales to the origin of the crown group. It is possible, however, that parallel trends in cranial telescoping independently evolved in some early odontocetes clades. Such a parallel trend is suggested by PC 1 scores in Xenorophidae, one of the earliest diverging clades of odontocete whales (Churchill et al. 2016; Geisler et al. 2014; Godfrey et al. 2016; Uhen 2008). Xenorophids are a relatively diverse clade of Oligocene whales known only from South and North Carolina (Uhen 2008), with many taxa yet to be described (Sanders and Geisler 2015). They are unique amongst odontocetes in having a large and prominent ascending process of the lacrimal overlapping the lateral portion of the frontal and a premaxilla underlapping the ascending processes of the maxilla. Within our PCA analysis, *Cotylocara* is recovered as having a more advanced degree of telescoping than that exhibited by either *Xenorophus* or *Echovenator* (Figs. 4 and 5), due in part to greater expansion of the maxilla and premaxilla. Further evidence of a separate and parallel trend in cranial telescoping is provided by *Archaeodelphis* (Allen 1921), a taxon that is sometimes placed outside of Xenorophidae (Sanders and Geisler 2015), but has generally been considered to represent the earliest diverging lineage of this clade (Uhen 2008; Geisler et al. 2014; Churchill et al. 2016; Godfrey et al. 2016). While not included within our morphometric analysis, *Archaeodelphis* is notable for having minimal development of the ascending process of the maxillae (Allen 1921), unlike other xenorophids (Geisler et al. 2014). This suggests that Xenorophidae and stem odontocetes convergently developed more advanced forms of telescoping, even though some degree of expansion of the maxilla over the frontals was present in the common ancestor of all odontocetes.

Perhaps the single most bizarre whale to be included in our analysis is *Odobenocetops peruvianus*. *Odobenocetops* belongs to a monogeneric family known only from the Late Miocene and earliest Pliocene of Western South America (Muizon 1993a). *Odobenocetops* possesses a unusual combination of cranial features found in no other whale, including anteriorly positioned external nares and orbits, a dorsally exposed temporal region, absence of the palatal portion of the maxilla, and massive asymmetrical tusks, and may have been specialized for benthic suction

feeding (Muizon 1993b; Muizon and Domning 2002). This taxon was included within our analysis of the right side of the skull, where its unique morphology is reflected in its position as an extreme outlier for PCs 1–3.

Odobenocetops has been considered to be a delphinoid, and closely related to Monodontidae (Muizon 1993a; Murakami et al. 2012; Murakami et al. 2014), the family comprising narwhals and belugas. In contrast to these earlier studies, our phylogenetic analysis (Appendix C) places *Odobenocetops* outside of Delphinoidea, and within a large clade including many "kentriodontids," that is in turn the sister group to a clade composed of Inoidea and Delphinoidea, a finding previously suggested by Pyenson et al. (2013). Although our phylogenetic hypothesis differs with respect to the position of *Odobenocetops*, for the current study the most important point is there is a consensus that it is a crown odontocete.

Although *Odobenocetops* is a member of crown group Odontoceti, it has an unusually low PC 1 score, overlapping in morphospace with xenorophids in degree of cranial telescoping. Whereas it is tempting to suggest that cranial telescoping is irreversible within echolocating whales, *Odobenocetops* is a clear exception to this rule. The extreme modification of the skull of this taxon has resulted in far anterior displacement of the external nares, and a reduced amount of overlap between the frontal and maxilla. *Odobenocetops* is thus the only whale to show clear evidence of a reversal of cranial telescoping. The extreme modification of the skull suggests that the melon is either extremely reduced in size if not lost entirely, suggesting a loss in the ability to echolocate (Muizon 1993b). If soft tissue anatomy related to echolocation plays a major role in constraining telescoping and overall shape of the skull in odontocetes, then a loss of this sensory ability may explain why we see radical changes in Odobenocetopsidae as compared to other odontocete lineages. In this case, *Odobenocetops* may be an exception that proves the rule, and demonstrates the strength of functional constraints related to echolocation on cranial telescoping in toothed whales.

Another whale with highly unusual cranial anatomy included in this analysis is the pygmy sperm whale, *Kogia breviceps*, a member of the sperm whale clade Physeteroidea. *Kogia* has the lowest PC 1 of any extant odontocete, and is considered to be one of the most bizarre whales alive today. The skull of *Kogia* can be easily distinguished from that of other odontocetes by the extreme brevirostry, presence of a supracranial basin occupying much of the dorsal surface of the skull, loss of nasals, high asymmetry, particularly of the premaxillae, and enormous development of the lacrimal-jugal (Heyning 1989). Beyond the bony anatomy, physeteroids also are the only living odontocetes to lack a melon, instead possessing a spermaceti organ, and uniquely retain distinct left and right nasal tracks that lead to a single blowhole (Cranford 1999; Heyning 1989). Studies of the roles of skull and soft tissues of *Physeter* (Huggenberger et al. 2014; Song et al. 2017) and *Kogia* (Karol et al. 1978; Goold and Clarke 2000; Song et al. 2015; Thornton et al. 2015 suggest acoustic specializations linked to this unusual structure, but some of the unique cranial and soft tissue structures of the head of *Physeter* may be derived for ramming behaviors (Panagiotopoulou et al. 2016; Alam et al 2016) as well. The bizarre cranial morphology described above has resulted in *Kogia* having a significant influence on the identification of major sources of variation in our facial morphology dataset; *Kogia* forms an extreme outlier for PC 4 of the whole skull dataset and principle components 3, 4, and 6 for the half skull dataset.

Phylogenetic analyses generally support *Kogia*, along with *Physeter*, as the earliest diverging lineage of crown odontocete, within the clade Physeteroidae, sister to Synrhina, a clade comprising Platanistoidea, Ziphiidae, and Delphinida (Geisler et al. 2011; Churchill et al. 2016; Gatesy et al. 2013a; Hamilton et al. 2001; Lambert et al. 2017a). It is thus perhaps not surprising that of all extant odontocetes, *Kogia* consistently has the lowest PC 1 score, and appears to occupy a middle region of morphospace between odontocetes with lesser degrees of telescoping, such as Xenorophidae, *Simocetus*, and *Agorophius*, and taxa with more advanced telescoping, including waipatiid- and squalodont-like taxa and the remainder of crown Odontoceti.

DIVERSITY OF FACIAL MORPHOLOGY THROUGH TIME

The Oligocene is an important time period in whale evolution; it is characterized by the rapid radiation and diversification of both mysticetes and odontocetes (Gatesy et al. 2013; Marx and Fordyce 2015; Boessenecker et al. 2017), possibly linked to changes in global climate and circulation (Fordyce 1977; Steeman et al. 2009) and the development of novel traits that allowed whales to exploit new niches: baleen in mysticetes (Deméré et al. 2008; Pyenson 2017) and echolocation in odontocetes (Lindberg and Pyenson 2007; Pyenson 2017). Most work on disparity in whales during the Oligocene has focused on mysticetes, which attained their greatest disparity during this epoch (Marx and Fordyce 2015). At no other time period do we see the presence of such a wide diversity of feeding morphologies within Mysticeti, including raptorial predators (*Janjucetus;* Fitzgerald 2006, and *Fucaia*; Marx et al. 2015), benthic suction feeders (*Mammalodon;* Fitzgerald 2010), and filter feeders that relied on teeth (*Coronodon;* Geisler et al. 2017, although see Hocking et al. 2017) or baleen (Eomysticetidae; Boessenecker and Fordyce 2015) or possibly a combination of both (Aetiocetidae; Deméré et al. 2008).

Odontocete diversification during this time period is much less well known, partially hampered by many taxa still remaining undescribed (Uhen 2008). However, even with the described

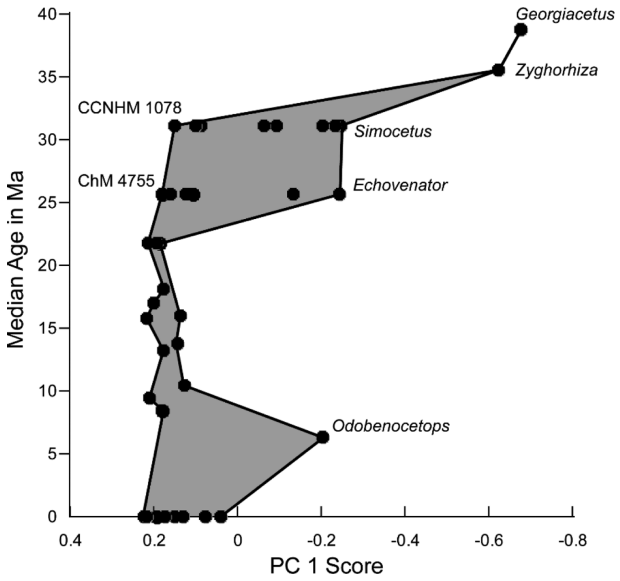

Figure 8. Disparity of archaeocete and odontocete PC 1 scores over time, based on age data presented in Table B2. Extreme outlier taxa labeled on the plot.

fossil record, there is still a substantial diversity in feeding morphology, including taxa adapted for raptorial feeding (*Waipatia*; Fordyce 1994), bottom-feeding (*Simocetus;* Fordyce 2002), and suction feeding (*Inermorostrum;* Boessenecker et al. 2017). Our study provides further evidence of the Oligocene being a time period of exceptional morphological diversity, in this case facial morphology.

When PC 1 scores are used as a proxy for cranial telescoping and are plotted against age (Fig. 8), the Oligocene is found to have the greatest disparity, as measured by PC score range. These taxa include representatives of all three grades of cranial telescoping outlined in this article. Most of these taxa are from the Oligocene Ashley and Chandler Bridge formations, suggesting that members of different telescoping stages may have been contemporaneous with each other (Appendix E), alongside tooth- and baleen-bearing mysticetes. In contrast, by the Miocene, nearly all this variation in odontocete PC 1 scores is lost, and PC 1 variability remains limited throughout the Neogene, with the exception of *Odobenocetops* in the late Miocene and early Pliocene. While our sampling of fossil taxa from the Miocene through Pliocene is limited, we doubt further sampling of Miocene fossil whales would significantly alter this pattern, as described taxa generally fall within the range of cranial telescoping morphologies found within the crown group. It is not clear why odontocete taxa with lower PC 1 scores and less advanced cranial telescoping did not survive the Oligocene, however it is possible that the more posteriorly displaced external nares of later diverging odontocetes may have provided some sort of increased energetic efficiency during breathing bouts on the surface, or that advanced cranial telescoping may be associated with changes in the soft anatomy that made these taxa better at echolocation. It is also possible that the extinction of taxa with less advanced cranial telescoping maybe coincidental and later diverging odontocetes acquired some other behavioral or morphological novelty that allowed them to outcompete other odontocetes. As demonstrated in this study, there is still much to learn about early odontocete diversity. Further analyses of morphological variation in early fossil whales will only grow our understanding of the breadth of adaptations and specializations the first odontocete whales possessed, and provide more detail on how the bizarre and unique features of the whale skull evolved.

AUTHOR CONTRIBUTIONS

Conceived and designed the study: MC, JHG, BLB, AG. Collected the data: MC. Analyzed the data: MC, JHG, BLB. Contributed material and expertise: MC, JHG, BLB, AG. Wrote the paper: MC, JHG, BLB, AG.

ACKNOWLEDGMENTS

For access to specimens, we would like to thank S. and R. Boessenecker, and P. Manning (CCNHM); M. Gibson and J. Peragine (ChM); J. Ososky, D. Bohaska, N. Pyenson, and C. Peredo (USNM), N. Simmons, E. Westwig, and E. Hoeger (AMNH), T. Deméré, K. Randall, and P. Unitt (SDNHM), and M. Riven (UWBM). For assistance with analyses, we thank D. Fraser (NMC), A. Cuff (RVC), T. Halliday (UCL), R. Felice (UCL), and M. Randau (UCL). We also acknowledge M. Uhen (GMU) for his contributions of age data to the Paleobiology database. For help with scanning of specimens, we thank J. Miguel (NYIT). Funding was provided by NSF-DEB 1349697 and the American Association of Anatomists. We also thank Samantha Hopkins, Olivier Lambert, and two anonymous reviewers for their helpful comments on this manuscript.

DATA ARCHIVING

Data available at https://doi.org/10.5061/dryad.6s268n1. Available stl files of 3d scans of whale skulls can be found on phenome10k (http://phenome10k.org).

LITERATURE CITED

Adams, D. C. 2014. A generalized *K* statistic for estimating phylogenetic signal from shape and other high-dimensional multivariate data. Syst. Biol. 63:685–697.

Adams, D. C., and E. Otarola-Castillo. 2013. Geomorph: an R package for the collection and analysis of geometric morphometric shape data. Methods Ecol. Evol. 4:393–399.

Aguirre-Fernández, G., and R. E. Fordyce. 2014. *Papahu taitapu*, gen. et sp. nov., an Early Miocene stem odontocete (Cetacea) from New Zealand. J. Vertebrate Paleontol. 34:195–210.

Alam, P., S. Aminib, M. Tadayon, A. Miserez, A. Chinsamy. 2016. Properties and architecture of the sperm whale skull amphitheatre. Zoology 119: 42–51.

Allen, G. M. 1921. A new fossil cetacean. Bull. Museum Comp. Zool. 65: 1–14.

Au, W. W. L., R. A. Kastelein, K. J. Benoit-Bird, T. W. Cranford, and M. F. McKenna. 2006. Acoustic radiation from the head of echolocating harbor porpoises (*Phocoena phocoena*). J. Exp. Biol. 209:2726–2733.

Bapst, D. W. 2012. Paleotree: an R package for paleontological and phylogenetic analyses of evolution. Methods Ecol. Evol. 3:803–807.

Berta, A., E. G. Ekdale, and T. W. Cranford. 2014. Review of the cetacean nose: form, function, and evolution. Anat. Rec. 297:2205–2215.

Boersma, A. T., and N. D. Pyenson. 2016. *Arktocara yakataga*, a new fossil odontocete (Mammalia, Cetacea) from the Oligocene of Alaska and the antiquity of Platanistoidea. PeerJ 4:e2321.

Boessenecker, R. W., and R. E. Fordyce. 2015. Anatomy, feeding ecology, and ontogeny of a transitional baleen whale: a new genus and species of Eomysticetidae (Mammalia: Cetacea) from the Oligocene of New Zealand. PeerJ 3:e1129.

Boessenecker, R. W., D. Fraser, M. Churchill, and J. H. Geisler. 2017. A toothless dwarf dolphin (Odontoceti: Xenorophidae) points to explosive feeding diversifaction of modern whales (Neoceti). Proc. R Soc. B 284:20170531.

Bookstein, F. L. 1997. Landmark methods for forms without landmarks: morphometrics of group differences in outline shape. Med. Image Anal. 1:225–243.

Butler, M. A., and A. A. King. 2004. Phylogenetic comparative analysis: a modeling approach for adaptive evolution. Am. Nat. 164:683–695.

Churchill, M., M. R. Martinez, C. Muizon, J. H. Geisler, and J. Mnieckowski. 2016. The origin of high frequency hearing in whales. Curr. Biol. 16:2144–2149.

Cranford, T. W. 1999. The sperm whale's nose: sexual selection on a grand scale? Marine Mammal Sci. 15:1133–1157.

Deméré, T. A., M. R. McGowen, A. Berta, and J. Gatesy. 2008. Morphological and molecular evidence for a stepwise evolutionary transition from teeth to baleen in mysticete whales. Syst. Biol. 57:15–37.

Felsensein, J. 1973. Maximum likelihood estimation of evolutionary trees from continuous characters. Am. J. Hum. Genet. 25:471–492.

Felsenstein, J. 1985. Phylogenies and the comparative method. Am. Nat. 125:1–15.

Fitzgerald, E. M. 2006. A bizarre new toothed mysticete (Cetacea) from Australia and the early evolution of baleen whales. Proc. R Soc. B Biol. Sci. 273:2955–2963.

———. 2010. The morphology and systematics of *Mammalodon colliveri* (Cetacea: Mysticeti), a toothed mysticete from the Oligocene of Australia. Zool. J. Linnean Soc. 158:367–476.

Fordyce, R. E. 1977. The development of the circum-Antarctic current and the evolution of the Mysticeti (Mammalia: Cetacea). Palaeogeogr. Palaeoclimatol. Palaeoecol. 21:265–271.

———. 1980. Whale evolution and Oligocene southern ocean environments. Palaeogeogr. Palaeoclimatol. Palaeoecol. 31:319–336.

———. 1994. *Waipatia maerewhenua* new genus and new species (Waipatiidae, new family), an archaic late Oligocene dolphin (Cetacea: Odontoceti: Platanistoidea) from New Zealand. Pp. 147–176 *in* A. Berta and T. A. Deméré, eds. Contributions in marine mammal paleontology honoring Frank C. Whitmore, Jr. San Diego Natural History Society, San Diego.

———. 2002. *Simocetus rayi* (Odontoceti: Simocetidae, new family): a bizarre new archaic Oligocene dolphin from the eastern North Pacific. Smithsonian Contrib. Paleobiol. 93:185–222.

Fordyce, R. E., and C. Muizon. 2001. Evolutionary history of cetaceans: a review. Pp. 169–232 *in* J. M. Mazin and V. de Buffrénil, eds. Secondary adaptation of tetrapods to life in water. Verlag Dr. Friedrich Pfeil, München.

Gatesy, J., J. H. Geisler, J. Chang, C. Buell, A. Berta, R. Meredith, M. S. Springer, and M. R. McGowen. 2013. A phylogenetic blueprint for a modern whale. Mol. Phylogenet. Evol. 66:479–506.

Geisler, J. H., R. W. Boessenecker, M. Brown, and B. L. Beatty. 2017. The origin of filter feeding in whales. Curr. Biol. 27:1–7.

Geisler, J. H., M. W. Colbert, and J. L. Carew. 2014. A new fossil species supports an early origin for toothed whale echolocation. Nature 508:383–386.

Geisler, J. H., M. R. McGowen, G. Yang, and J. Gatesy. 2011. A supermatrix analysis of genomic, morphological, and paleontological data from crown Cetacea. BMC Evol. Biol. 11:112.

Geisler, J. H., and A. E. Sanders. 2003. Morphological evidence for the phylogeny of Cetacea. J. Mammalian Evol. 10:23–129.

Godfrey, S. J. 2013. On the olfactory apparatus in the Miocene odontocete *Squalodon* sp. (Squalodontidae). Comptes Rendus Palevol. 12:519–530.

Godfrey, S., M. D. Uhen, J. E. Osborne, and L. E. Edwards. 2016. A new specimen of *Agorophius pygmaeus* (Agorophiidae, Odontoceti, Cetacea) from the early Oligocene Ashley formation of South Carolina, USA. J. Paleontol. 90:154–169.

Goold, J. C., and Clarke, M. R. 2000. Sound velocity in the head of the dwarf sperm whale, *Kogia sima*, with anatomical and functional discussion. J. Marine Biol. Assoc. United Kingdom 80:535–542.

Gunz, P., P. Mitteroecker, and F. L. Bookstein. 2005. Semilandmarks in three dimensions. Pp. 73–98 *in* D. E. Slice, ed. Modern morphometrics in physical anthropology. Springer, Berlin.

Hamilton, H., S. Caballero, A. G. Collins, and R. L. Brownell. 2001. The evolution of river dolphins. Proc. R Soc. Lond. Ser. B 268:549–556.

Harmon, L. J., J. B. Losos, T. Jonathan Davies, R. G. Gillespie, J. L. Gittleman, W. Bryan Jennings, K. H. Kozak, M. A. McPeek, F. Moreno-Roark, T. J. Near, and A. Purvis. 2010. Early bursts of body size and shape evolution are rare in comparative data. Evolution 64:2385–2396.

Harmon, L. J., J. T. Weir, C. D. Brock, R. E. Glor, and W. Challenger. 2008. GEIGER: investigating evolutionary radiations. Bioinformatics 24:129–131.

Heyning, J. E. 1989. Comparative facial anatomy of beaked whales (Ziphiidae) and a systematic revision among the families of extant Odontoceti. Contributions in Science, Natural History Museum of Los Angeles County 464:1–64

Heyning, J. E., and J. G. Mead. 1990. Evolution of the nasal anatomy of cetaceans. Pp. 67–79 *in* J. A. Thomas and R. A. Kastelein, eds. Sensory abilities of Cetaceans. New York, Springer.

Hocking, D. P., F. G. Marx, E. M. G. Fitzgerald, and A. R. Evans. 2017. Ancient whales did not filter feed with their teeth. Biol. Lett. 13. pii: 20170348.

Huggenberger, S., M. Andre', and H. H. A. Oelschläger. 2014. The nose of the sperm whale: overviews of functional design, structural homologies and evolution. J. Marine Biol. Assoc. United Kingdom 96: 783–806.

Karol, R., C. Litchfield, D. K. Caldwell, and M. C. Caldwell. 1978. Compositional topography of melon and spermaceti organ lipids in the pygmy sperm whale *Kogia breviceps*: implications for echolocation. Marine Biol. 47:115–123.

Klima, M. 1999. Development of the cetacean nasal skull. Springer, Berlin.

Lambert, O., G. Bianucci, M. Urbina, and J. H. Geisler. 2017a. A new inioid (Cetacea, Odontoceti, Delphinida) from the Miocene of Peru and the origin of modern dolphin and porpoise families. Zool. J. Linnean Soc. 179:919–946.

Lambert, O., M. Martinez-Cáceres, G. Bianucci, C. Di Celma, R. Salas-Gismondi, E. Steurbaut, M. Urbina, and C. Muizon. 2017b. Earliest Mysticete from the Late Eocene of Peru sheds new light on the origin of baleen whales. Curr. Biol. 27:1535–1541.

Lambert, O., G. Bianucci, and M. Urbina. 2014. *Huaridelphis raimondii*, a new early Miocene Squalodelphinidae (Cetacea, Odontoceti) from the Chilcatay Formation, Peru. J. Vertebrate Paleontol. 34:897–1004.

Lambert, O., G. Bianucci, M. Urbina, and J. H. Geisler. 2017. A new inioid (Cetacea, Odontoceti, Delphinida) from the Miocene of Peru and the

origin of modern dolphin and porpoise families. Zool. J. Linnean Soc. 179:919–946.

Lambert, O., C. Muizon, and G. Bianucci. 2015. A new archaic homodont cetacean (Mammalia, Cetacea, Odontoceti) from the early Miocene of Peru. Geodiversitas 37:79–108.

Lindberg, D. R., and N. D. Pyenson. 2007. Things that go bump in the night: evolutionary interactions between cephalopods and cetaceans in the tertiary. Lethaia 40: 335–343.

Marx, F. G., and R. E. Fordyce. 2015. Baleen boom and bust: a synthesis of mysticete phylogeny, diversity, and disparity. Royal Soc. Open Sci. 2:140434.

Marx, F. G., O. Lambert, and M. D. Uhen. 2016. Cetacean paleobiology. John Wiley & Sons, Chichester, U. K.

Marx, F. G., C. H. Tsai, and R. E. Fordyce. 2015. A new early Oligocene toothed "baleen" whale (Mysticeti: Aetiocetidae) from western North America: one of the oldest and smallest. Royal Soc. Open Sci. 2:150476.

McGowen, M. R. 2011. Toward the resolution of an explosive radiation—a multilocus phylogeny of oceanic dolphins (Delphinidae). Mol. Phylogenet. Evol. 60:345–357.

McGowen, M. R., M. Spaulding, and J. Gatesy. 2009. Divergence date estimation and a comprehensive molecular tree of extant cetaceans. Mol. Phylogenet. Evol. 53:891–906.

McKenna, M. F., T. W. Cranford, A. Berta, and N. D. Pyenson. 2012. Morphology of the odontocete melon and its implications for acoustic function. Marine Mammal Sci. 28:690–713.

Miller, G. S. J. 1923. The telescoping of the cetacean skull. Smithsonian Miscellaneous Collections 76:1–71.

Mitchell, E. D. 1989. A new cetacean from the Late Eocene La Meseta Formation, Seymour Island, Antarctic Penisula. Canadian J. Aquatic Sci. 46:2219–2235.

Muizon, C. 1993a. *Odobenocetops peruvianus*: una remarcable convergencia de adaptacion alimentaria entre morsa y delfin. Institut Francais d'Etudes Andines 22:671–683.

———. 1993b. Walrus-like feeding adaptation in a new cetacean from the Pliocene of Peru. Nature 365:745–748.

Muizon, C., and D. P. Domning. 2002. The anatomy of *Odobenocetops* (Delphinoidea, Mammalia), the walrus-like dolphin from the Pliocene of Peru and its palaeobiological implications. Zool. J. Linnean Soc. 134:423–452.

Murakami, M., C. Shimada, Y. Hikida, and H. Hirano. 2012. Two new extinct basal phocoenids (Cetacea, Odontoceti, Delphinoidea), from the upper Miocene Koetoi Formation of Japan and their phylogenetic significance. J. Vertebrate Paleontol. 32:1172–1185.

Murakami, M., C. Shimada, Y. Hikida, Y. Soeda, and H. Hirano. 2014. *Eodelphis kabatensis*, a new name for the oldest true dolphin *Stenella kabatensis* Horikawa, 1977 (Cetacea, Odontoceti, Delphinidae), from the Upper Miocene of Japan, and the phylogeny and paleobiogeography of Delphinoidea. J. Vert. Paleontol. 34:491–511.

Oelschläger, H. A. 1990. Evolutionary morphology and acoustics in the dolphin skull. Pp. 137–162 *in* J. A. Thomas and R. A. Kastelein, eds. Sensory abilities of Cetaceans. Plenum Press, New York.

———. 2000. Morphological and functional adaptations of the toothed whale head to aquatic life. Hist. Biol. 14:33–39.

Pagel, M. 1999. Inferring the historical patterns of biological evolution. Nature 401:877–884.

Panagiotopoulou, P., P. Spyridis, H. Mehari Abraha, D. R. Carrier, and T. C. Pataky. 2016. Architecture of the sperm whale forehead facilitates ramming combat. PeerJ 4:e1895.

Paradis, E., J. Claude, and K. Strimmer. 2004. APE: analyses of phylogenetics and evolution in R language. Bioinformatics 20:289–290.

Park, T., E. M. G. Fitzgerald, and A. R. Evans. 2016. Ultrasonic hearing and echolocation in the earliest toothed whales. Biol. Lett. 12:20160060.

Pyenson, N. D. 2017. The ecological rise of whales chronicled by the fossil record. Curr. Biol. 27:R558–R564.

Pyenson, N. D., C. S. Gutstein, M. A. Cozzuol, J. Velez-Juarbe, and M. Suárez. 2013. New material of *Odobenocetops* from the late Miocene of Chile clarifies the systematics and paleobiology of walrus-convergent odontocetes. Society of Vertebrate Paleontology annual meeting, Los Angeles, California, 2013.

Pyenson, N. D., and S. N. Sponberg. 2011. Reconstructing body size in extinct crown Cetacea (Neoceti) using allometry, phylogenetic methods, and tests from the fossil record. J. Mammalian Evol. 4:269–288.

Rauschmann, M. A., S. Huggenberger, L. S. Kossatz, and H. A. Oelschläger. 2006. Head morphology in perinatal dolpins: a window into phylogeny and ontogeny. J. Morphol. 267:1295–1315.

Raven, H. C., and W. K. Gregory. 1933. The spermaceti organ and nasal passages of the sperm whael (*Physeter catodon*) and other odontocetes. Am. Museum Novitates 667:1–8.

Revell, L. J. 2012. Phytools: an R package for phylogenetic comparative biology (and other things). Methods Ecol. Evol. 3:217–223.

Sanders, A. E., and J. H. Geisler. 2015. A new basal odontocete from the upper Rupelian of South Carolina, U.S.A., with contributions to the systematics of *Xenorophus* and *Mirocetus* (Mammalia, Cetacea). J. Vert. Paleontol. 35:e890107.

Schlager, S. 2017. Morpho and Rvcg—shape analysis in R. Pp. 217–256 *in* G. Zheng, S. Li, and G. Szekely, eds. Statistical shape and deformation analysis. Academic Press, Cambridge.

Schulte, H. V. W. 1917. The skull of *Kogia breviceps*. Bull. Am. Museum Nat. Hist. 37:361–404.

Song, Z., Xu, X., Dong, J., Xing, L, Zhang, M., Liu, X., Zhanga, Y., Li, S., and Berggren, P. 2015. Acoustic property reconstruction of a pygmy sperm whale (*Kogia breviceps*) forehead based on computed tomography imaging. J. Acoust. Soc. Am. 138:3129–3137.

Song, Z., Y. Zhang, S. W. Thornton, S. Li, and J. Dong. 2017. The influence of air-filled structures on wave propagation and beam formation of a pygmy sperm whale (*Kogia breviceps*) in horizontal and vertical planes. J. Acoust. Soc. Am. 142:2443–2453.

Steeman, M. E., M. B. Hebsgaard, R. E. Fordyce, S. Y. W. Ho, D. L. Rabosky, R. Nielsen, C. Rahbek, H. Glenner, M. V. Sørenson, and E. Willerslev. 2009. Radiation of extant cetaceans driven by restructuring of the oceans. Syst. Biol. 58:573–585.

Tanaka, Y., and R. E. Fordyce. 2014. Fossil dolphin *Otekaikea marplesi* (latest Oligocene, New Zealand) expands the morphological and taxonomic diversity of Oligocene cetaceans. PLoS ONE 9:e107972.

Tanaka, Y., and R. E. Fordyce. 2015. Historically significant late Oligocene dolphin *Microcetus hectori* Benham 1935: a new species of Waipatia (Platanistoidea). J. R Soc. New Zealand 45:135–150.

Tanaka, Y., and R. E. Fordyce. 2017. *Awamokoa tokarahi*, a new basal dolphin in the Platanistoidea (late Oligocene, New Zealand). J. Syst. Paleontol. 15:365–386.

Thornton, S. W., W. A. McLellan, S. A. Rommel, R. M. Dillaman, D. P. Nowacek, H. N. Koopman, and D. A. Pabst. 2015. Morphology of the Nasal Apparatus in Pygmy (Kogia Breviceps) and Dwarf (*K. sima*) sperm whales. Anat. Rec. 298:1301–1326.

Uhen, M. D. 2008. A new *Xenorophus*-like odontocete cetacean from the Oligocene of North Carolina and a discussion of the basal odontocete radiation. J. Syst. Paleontol. 6:433–452.

Weems, R. E., L. M. Bybell, L. E. Edwards, W. C. Lewis, J. M. Self-Trail, L. B. I. Albright, D. J. Cicimurri, W. B. Harris, J. E. Osborne, and

A. E. Sanders. 2016. Stratigraphic revision of the Cooper Group and Chandler Bridge and Edisto Formations in the coastal plain of South Carolina. South Carolina Geol. 49:1–24.

Whitmore, J. F. C., and A. E. Sanders. 1976. Review of Oligocene Cetacea. Syst. Zool. 25:304–320.

Wiley, D. F., N. Amenta, D. A. Alcanatara, D. Ghosh, Y. J. Kil, E. Delson, W. Harcourt-Smith, F. J. Rohlf, J. K. St, and B. Hamann. 2005. Evolutionary morphing. Proceedings of IEEE Visualization 2005 (VIS′05), Minneapolis, MN.

Associate Editor: S. Hopkins
Handling Editor: Mohamed A.F. Noor

Supporting Information

Additional supporting information may be found online in the Supporting Information section at the end of the article.

Appendix A. List of specimens examined for this study, organized by taxonomy.

Figure S1. Diversity of Oligocene fossil odontocetes known from the Charleston region of South Carolina, including both basal (**A**, *Xenorophus* sp., ChM PV4823) and late diverging xenorophids (**B**, *Cotylocara macei* CCNHM 101), "simocetid-like" stem odontocetes (**C**, CCNHM PV4178), agorophiids (**D**, *Agorophius pygmaeus* ChM PV4256), and waipatiid-(**E**, CCNHM 172) and squalodont-like (**F**, ChM PV7679) taxa.

Figure S2. Comparisons of landmark placement in dorsal view in a typical odontocete (**A**, *Tursiops truncatus* SDNHM 11102), as well as the same landmarks applied on an archaeocete skull (**B**, *Zygorhiza kochi* USNM 11962) and a kogiid skull (**C**, *Kogia breviceps* USNM 22015).

Figure S3. Skulls of 3 unnamed species of Oligocene cetaceans from the Charleston area: (**A**, unnamed *Waipatia-like* odontocete, represented by ChM PV4961 and CCNHM 172), (**B**, *Xenorophus* sp., represented by ChM PV4823 and CCNHM 104.1), and (**C**, agorophiid-like odontocete, represented by ChM PV5852 and CCNHM 209).

Figure S4. Results of phylogenetic analysis of total evidence character matrix, with a molecular constraint enforced.

Figure S5. Results of phylogenetic analysis of total evidence character matrix, with a molecular constraint enforced.